Acta Crystallographica Section B
Structural Science
ISSN 0108-7681

Structures and phase transitions of the A_7PSe_6 (A = Ag, Cu) argyrodite-type ionic conductors. III. α-Cu_7PSe_6

E. Gaudin,[a] V. Petricek,[b] F. Boucher,[a] F. Taulelle[c] and M. Evain[a]*

[a]Laboratoire de Chimie des Solides, IMN, UMR C6502 CNRS, Université de Nantes, 2 rue de la Houssinière, BP 32229, 44322 Nantes CEDEX 3, France, [b]Institute of Physics, Academy of Sciences of the Czech Republic, Na Slovance 2, 180 40 Praha 8, Czech Republic, and [c]RMN et Chimie du Solide, UMR 7510, Université Louis Pasteur, 4 rue Blaise Pascal, 67070 Strasbourg CEDEX, France

Correspondence e-mail: evain@cnrs-imn.fr

Received 15 May 2000
Accepted 24 July 2000

The crystal structure of the third polymorph of the Cu_7PSe_6 argyrodite compound, α-Cu_7PSe_6, heptacopper phosphorus hexaselenide, is determined by means of single-crystal diffraction from twinned crystals and X-ray powder diffraction, with the help of extensive NMR measurements. In the low-temperature form, *i.e.* below the last phase transition, α-Cu_7PSe_6 crystallizes in orthorhombic symmetry, space group $Pna2_1$, with a = 14.3179 (4), b = 7.1112 (2), c = 10.1023 (3) Å, V = 1028.590 (9) Å^3 (deduced from powder data, T = 173 K) and Z = 4. Taking into account a twinning by reticular merohedry, the refinement of the α-Cu_7PSe_6 structure leads to the residual factors R = 0.0466 and wR = 0.0486 for 127 parameters and 3714 observed, independent reflections (single-crystal data, T = 173 K). A full localization of the Cu^+d^{10} element is reached with one twofold-, one threefold- and five fourfold-coordinated Cu atoms. The observation of two phase transitions for Cu_7PSe_6, to be compared with only one for Ag_7PSe_6, is attributed to the d^{10} element stability in a low coordination environment, copper being less prone to lower coordination sites than silver, especially at low temperature.

1. Introduction

To apprehend and rationalize the phase transitions observed in the argyrodite-type ionic conductors, several studies were initiated in the A_7PSe_6 (A = Ag, Cu) systems. The choice of these two systems is twofold. First, in the argyrodite family some compounds, *e.g.* Ag_7PSe_6, present only one phase transition, other compounds, such as Cu_7PSe_6, exhibit on the contrary two phase transitions. Second, these two systems present nuclei which are practical for NMR (^{107}Ag, ^{63}Cu, ^{31}P and ^{77}Se) and crucial in the structure determination process.

In part I of our study (Evain *et al.*, 1998), we focused on the Ag_7PSe_6 system. From the X-ray structure determination of both the β-Ag_7PSe_6 and γ-Ag_7PSe_6 polymorphic forms, the $\gamma \rightarrow \beta$ phase transition could be analyzed in terms of cation ordering. Indeed, using a combination of a non-harmonic Gram–Charlier expansion of the Debye–Waller factors (DWFs) and a split model, the diffusion paths of Ag^+ were evidenced in the γ-Ag_7PSe_6 high-temperature polymorphic form. Also, a clear localization of those Ag^+d^{10} cations in the most pronounced probability density areas of the diffusion paths was observed at the phase transition towards the β-Ag_7PSe_6 low-temperature polymorphic form. These preferential sites were of various types, *e.g.* linear, triangular or tetrahedral, as usually observed for Ag^+ in chalcogenides.

In part II of our study (Gaudin, Boucher, Petricek *et al.*, 2000), we initiated the structure determination of two of the

three polymorphic forms of Cu_7PSe_6: γ-Cu_7PSe_6 and β-Cu_7PSe_6. As in the Ag_7PSe_6 system, the most effective diffusion paths of the d^{10} species in the γ-Cu_7PSe_6 ionic conducting phase could be identified using a non-harmonic development of the DWFs in combination with a split model. Once again, at the phase transition at 320 K, when lowering the temperature towards β-Cu_7PSe_6, an ordering of the Cu^+d^{10} cations was observed, but, contrary to the Ag_7PSe_6 case, this ordering was incomplete. In particular, one copper position (Cu2) was distributed in β-Cu_7PSe_6 over two self-excluding positions (Cu2*a* and Cu2*b*, tetrahedral and triangular-like, respectively) and another copper (Cu3, linearly coordinated) showed a probability density function spread over a large area. It was therefore suspected that the second transition at 250 K could be related to a final resolution of the remaining disorder and a displacement of the linearly coordinated Cu atom towards much more stable triangular or tetrahedral sites.

In this last part of our study, we report the X-ray single-crystal structure determination of α-Cu_7PSe_6, the lowest-temperature polymorphic form of Cu_7PSe_6. The structure determination was not included in Part II of this series (Gaudin, Boucher, Petricek *et al.*, 2000) because of its complexity. Indeed, the final structural model could not be established without the results of extensive NMR measurements, both on powders and large single crystals. Notice that only the important NMR results, critical for the structure determination, will be exposed in this report; the detailed MAS NMR measurements and analyses will appear in a separate publication (Gaudin, Evain *et al.*, 2000).

2. Experimental

The synthesis and characterization of Cu_7PSe_6 has already been reported in part II of our study (Gaudin, Boucher, Petricek *et al.*, 2000). Out of the three single crystals used for the structure determination of β-Cu_7PSe_6 (labeled RT1, RT2 and RT3), only one (RT1) could be used for the low-temperature measurements (the RT2 and RT3 crystals were actually damaged in high-temperature measurements). It is important to mention that the RT1 crystal was twinned by merohedry at room temperature (β-Cu_7PSe_6 form), with a 24.1% twin fraction. To carry out the structure determination of α-Cu_7PSe_6 (see below), a fourth crystal with a twin fraction as low as possible at room temperature was searched. A crystal, shaped as a sphere by means of an air-blowing abrasive device, was found with a twin fraction below 2%. For simplicity, the two crystals that were effectively used at low temperature will be thereafter labeled LT1 (RT1) and LT2 (new crystal).

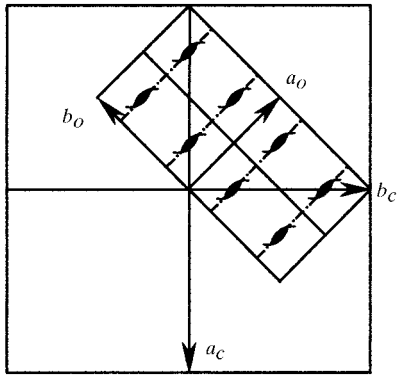

Figure 1
Cubic to orthorhombic (LT1, see text) cell transformation.

2.1. LT1 study

The data collection on LT1 (sphere 0.086 mm in radius) was carried out on a Siemens P4 diffractometer using graphite-monochromated Ag radiation (λ = 0.5609 Å) at 213 K, which is *ca* 40 K below the $\beta \rightarrow \alpha$ transition. The 213 K temperature was achieved using the original Siemens low-temperature nitrogen gas-blowing equipment and controlled within a 1 K range. The lattice was apparently cubic with unit-cell parameter $a \simeq 10.1$ Å. Data processing and all refinements were performed with the *JANA*2000 program package (Petricek & Dusek, 1998). Scattering factors and anomalous dispersion correction terms were taken from Maslen *et al.* (1992) and Creagh & McAuley (1992), respectively. After the usual data correction (Lorentz–polarization and intensity decay), the intensities were corrected for absorption by means of a spherical model.

From the analysis of the set of intensities, the highest symmetry point group appeared to be $\bar{4}3m$ [$R_{\rm int}(I)$ = 5.8%]. However, subsequent ^{77}Se MAS NMR and single-crystal ^{31}P NMR studies (Gaudin, Evain *et al.*, 2000), carried out to clarify the apparent symmetry contradictions (the α-Cu_7PSe_6 phase having a higher symmetry than β-Cu_7PSe_6), clearly showed the loss of cubic symmetry. Comparison of the collected NMR spectra with the ^{77}Se spectra of several argyrodite phases suggested an orthorhombic symmetry, with $Pmn2_1$ as a possible space group. A possible twinning had therefore to be imagined. To generate the $\bar{4}3m$ point group from the *mm*2 subgroup, six twin laws are required, for instance: *E*, 3[111], 3^2[111], $\bar{4}$[001], $\bar{4}$[010] and *m*[011] (herein labeled *T*1, *T*2, *T*3, *T*4, *T*5 and *T*6, respectively; see Table 1[1]). The orthorhombic cell ($a \simeq b \simeq 7.1$ and $c \simeq 10.1$ Å) was derived from the cubic cell (see Fig. 1) through the following transformation matrix

$$U = \begin{pmatrix} -1/2 & -1/2 & 0 \\ 1/2 & -1/2 & 0 \\ 0 & 0 & 1 \end{pmatrix}.$$

Taking into account the twin laws, all reflections could be indexed with the new cell and agreed with the $Pmn2_1$ space group (notice that the systematic absences are not systematically verified due to the twinning by reticular merohedry). However, although a complete diffraction sphere was considered, the reflections could not be averaged since the only symmetry element of the *mm*2 point group which is an invariant subgroup of $\bar{4}3m$ is the identity *E* (see annex).

[1] Supplementary data for this paper are available from the IUCr electronic archives (Reference: LC0028). Services for accessing these data are described at the back of the journal.

Table 1
Twinning matrix Tx calculated from $Tx = P^{-1}RxP$.

The twinning matrices correspond to the *hkl* indices defined as row vectors.

	Cubic cell ($\bar{4}3m$)		Orthorhombic cell ($mm2$)	
	$a \simeq 10.1$ Å		$a \simeq 7.1$ Å $b \simeq 7.1$ Å $c \simeq 10.1$ Å	$a \simeq 14.2$ Å $b \simeq 7.1$ Å $c \simeq 10.1$ Å
Transformation matrix		P	$\begin{pmatrix} -1/2 & -1/2 & 0 \\ 1/2 & -1/2 & 0 \\ 0 & 0 & 1 \end{pmatrix}$	$\begin{pmatrix} -1 & -1/2 & 0 \\ -1 & 1/2 & 0 \\ 0 & 0 & -1 \end{pmatrix}$
Twinning matrices				
R1: E	$\begin{pmatrix} 1 & 0 & 0 \\ 0 & 1 & 0 \\ 0 & 0 & 1 \end{pmatrix}$	$T1$	$\begin{pmatrix} 1 & 0 & 0 \\ 0 & 1 & 0 \\ 0 & 0 & 1 \end{pmatrix}$	$\begin{pmatrix} 1 & 0 & 0 \\ 0 & 1 & 0 \\ 0 & 0 & 1 \end{pmatrix}$
R2: 3 [111]	$\begin{pmatrix} 0 & 0 & 1 \\ 1 & 0 & 0 \\ 0 & 1 & 0 \end{pmatrix}$	$T2$	$\begin{pmatrix} -1/2 & -1/2 & -1 \\ 1/2 & 1/2 & -1 \\ 1/2 & -1/2 & 0 \end{pmatrix}$	$\begin{pmatrix} 1/2 & 1/4 & 1/2 \\ -1 & -1/2 & 1 \\ 1 & -1/2 & 0 \end{pmatrix}$
R3: 3^2[111]	$\begin{pmatrix} 0 & 1 & 0 \\ 0 & 0 & 1 \\ 1 & 0 & 0 \end{pmatrix}$	$T3$	$\begin{pmatrix} -1/2 & 1/2 & 1 \\ -1/2 & 1/2 & -1 \\ -1/2 & -1/2 & 0 \end{pmatrix}$	$\begin{pmatrix} 1/2 & -1/4 & 1/2 \\ 1 & -1/2 & -1 \\ 1 & 1/2 & 0 \end{pmatrix}$
R4: $\bar{4}$[001]	$\begin{pmatrix} 0 & 1 & 0 \\ -1 & 0 & 0 \\ 0 & 0 & -1 \end{pmatrix}$	$T4$	$\begin{pmatrix} 0 & 1 & 0 \\ -1 & 0 & 0 \\ 0 & 0 & -1 \end{pmatrix}$	$\begin{pmatrix} 0 & -1/2 & 0 \\ 2 & 0 & 0 \\ 0 & 0 & -1 \end{pmatrix}$
R5: $\bar{4}$[010]	$\begin{pmatrix} 0 & 0 & -1 \\ 0 & -1 & 0 \\ 1 & 0 & 0 \end{pmatrix}$	$T5$	$\begin{pmatrix} -1/2 & 1/2 & 1 \\ 1/2 & -1/2 & 1 \\ -1/2 & -1/2 & 0 \end{pmatrix}$	$\begin{pmatrix} -1/2 & 1/4 & -1/2 \\ 1 & -1/2 & -1 \\ 1 & 1/2 & 0 \end{pmatrix}$
R6: m[011]	$\begin{pmatrix} 1 & 0 & 0 \\ 0 & 0 & -1 \\ 0 & -1 & 0 \end{pmatrix}$	$T6$	$\begin{pmatrix} 1/2 & 1/2 & -1 \\ 1/2 & 1/2 & 1 \\ -1/2 & 1/2 & 0 \end{pmatrix}$	$\begin{pmatrix} 1/2 & 1/4 & -1/2 \\ 1 & 1/2 & 1 \\ -1 & 1/2 & 0 \end{pmatrix}$

A first model was built from the atomic positions of γ-Cu_7PSe_6, the high-temperature polymorphic form. Indeed, the orthorhombic $Pmn2_1$ space group derives directly from $F\bar{4}3m$, but not from the $P2_13$ space group of the intermediate β-Cu_7PSe_6 phase. Starting from the [PSe_6] structural skeleton and using the isotropic displacement parameter (IDP), the residual factor converged to $R = 0.24$. Some twinning fractions ($T2$ and $T5$) had to be fixed to zero to prevent negative values. To locate the Cu atoms, several sets of positions were deduced from the copper mode positions of the γ-Cu_7PSe_6 high-temperature form and tested. This is not a straightforward procedure, because of the featureless character of the Fourier difference maps and the numerous refinement local minima. After many attempts, a solution with split positions for some Cu atoms was found and the residual factor reached the value $R = 0.042$ (see Table 2). The atomic displacements could not be described anisotropically, because of non-positive definite tensors, but the freed twin fractions converged towards positive values (0.13, 0.17, 0.18, 0.14, 0.18 and 0.20 for T1, T2, T3, T4, T5 and T6, respectively). Given the particular arrangement of the split copper positions (mirror symmetry), a possible supercell was envisioned and powder diffraction studies were initiated.

2.2. Powder diffraction

Diffractograms were collected in the 213–350 K temperature range on two different Siemens D5000 powder diffractometers, one equipped with an Elphyse PSD detector and an Anton Parr (TTK) chamber and the other one equipped with a Kevex (2005–212) detector and the same temperature apparatus. The latter detector was necessary to observe the relatively small orthorhombic distortion. The powder pattern of the low-temperature phase could be fully indexed with a cell twice as large ($a \simeq 7.1$, $b \simeq 14.3$ and $c \simeq 10.1$ Å) as that derived from the original cubic lattice. New data collections on single crystals were then planned on an image plate equipped Stoe diffractometer (see below). Besides, a Le Bail-type fit (Le Bail *et al.*, 1988) of all the diffractograms with the *GSAS* program (Larson & Von Dreele, 1994) provided the cell parameter and volume evolution presented in Fig. 2.

2.3. LT2 study

The new crystal (LT2), which was smaller than the original LT1 crystal, was used for the Stoe IPDS recording. The data collection was carried out at 173 K in a low-resolution mode (IP at 60 mm) with rather long exposure times (8 min) to accurately measure weak reflection intensities. The integration was realised on the basis of the apparent cubic cell ($a \simeq 20.2$ Å) and the intensities were corrected from absorption using a spherical model. The orthorhombic cell was then derived from the cubic cell through the following matrix

$$U' = \begin{pmatrix} -1/4 & -1/2 & 0 \\ 1/4 & -1/2 & 0 \\ 0 & 0 & 1/2 \end{pmatrix}.$$

With the six twin laws, modified to take into account the cell change (see Table 1), the set of 35 596 measured reflections could be indexed and the intensities averaged for redundancy only (see above). Then, 29 369 reflections were available. Starting from the solution found in the subcell (space group $Pmn2_1$), an ordered structural model was envisaged in the supercell with $Pbn2_1$ as the space group ($Pbn2_1$ being a subgroup of the lower index of the $Pmn2_1$ space group). The space group was thereafter changed to the $Pna2_1$ standard setting. Notice that the refinements were carried out on F with

Table 2
Crystal, X-ray data collection and refinement parameters for Cu_7PSe_6.

	α-Cu_7PSe_6	
Physical, crystallographic and analytical data		
Formula	Cu_7PSe_6	
Mol. wt (g mol^{-1})	949.56	
Crystal system	Orthorhombic	
Space group	$Pmn2_1$(31)	$Pna2_1$(33)
No. of reflections for cell parameter determination	34	
a (Å)	7.1426 (8)†	14.3179 (4)‡
b (Å)†	7.1426 (8)†	7.1112 (2)‡
c (Å)†	10.1012 (11)†	10.1023 (3)‡
V (Å^3)†	515.33 (6)†	1028.590 (9)‡
Z	2	4
Density (calc., g cm^{-3})	6.118	6.117
Crystal description	Sphere	
Crystal size (mm)	0.086 (radius)	0.065 (radius)
Crystal color	Metallic luster	
Data collection		
Temperature (K)	213	173
Diffractometer	Siemens P4	Stoe IPDS
Radiation	Ag $KL_{2,3}$ (0.56087 Å)	Mo $KL_{2,3}$ (0.71073 Å)
Monochromator	Oriented graphite (002)	
Scan mode	ω	ω
hkl range	$-9 < h < 8$	$-18 < h < 18$
	$-10 < k < 8$	$-9 < k < 9$
	$-16 < l < 16$	$-13 < l < 13$
Sin θ/λ range (Å^{-1})	0.822	0.65
No. of standard reflections	3	–
Frequency of standard reflections (s)	3600	–
Data reduction		
Linear absorption coefficient (cm^{-1})	186.67	352.91
Absorption correction	Spherical method	
T_{min}/T_{max}	0.1130/0.1365	0.0527/0.1447
No. of reflections	3463	37639
No. of independent reflections	1719	29 369
Criterion for observed reflections	$I > 3.0\sigma(I)$	$I > 3.0\sigma(I)$
No. of observed reflections	946	3714
Refinement results		
Refinement	F	F
F(000)	844	1688
No. of reflections used in the refinement	946	3714
R§	0.0423	0.0466
wR§	0.0481	0.0486
S§	1.59	1.06
No. of refined parameters	51	127
$(\Delta/\sigma)_{max}$	< 0.0001	< 0.0001
Extinction coefficient¶	–	0.019 (2)
Weighting scheme	$w = 1/[\sigma^2\|F^o\| + (0.01\|F^o\|)^2]$	$w = 1/[\sigma^2\|F^o\| + (0.02\|F^o\|)^2]$
Difference Fourier residues (e Å^{-3})	[−1.36, +1.92]	[−2.03, +2.25]

† Deduced from the observed cubic cell ($P4$, 213 K). ‡ Deduced from the powder X-ray diffraction patterns (173 K). § $R = \Sigma||F_o| - |F_c||/\Sigma|F_o|$; $wR = [\Sigma w(|F_o| - |F_c|)^2/\Sigma w|F_o|^2]^{1/2}$; $S = [\Sigma w(|F_o| - |F_c|)^2/(N - M)]^{1/2}$. ¶ Isotropic secondary extinction (Type I) Gaussian distribution (Becker & Coppens, 1974).

all reflections included (the set of 29 369 *hkl*), although the R values hereinafter reported are given only for the observed reflections [3714 reflections with $I > 3\sigma(I)$]. With IDPs for all atoms the residual factor smoothly converged to the value R = 0.054. Introducing anisotropic displacement parameters (ADPs) for all atoms, except the P atom, and an isotropic secondary extinction coefficient (Becker & Coppens, 1974), the final residual factor was established as R = 0.046 (wR = 0.048) for 127 parameters. A difference Fourier synthesis then

Table 3
Fractional atomic coordinates, equivalent isotropic displacement parameters (Å^2) and s.u.s for α-Cu_7PSe_6 ($Pna2_1$, T = 173 K).

$$U_{eq} = \Sigma_i\Sigma_j U^{ij}a^i a^j \mathbf{a}_i\mathbf{a}_j.$$

	x	y	z	U_{eq}
P	0.1239 (3)	0.7531 (6)	1/4	0.0027 (4)
Se1a	0.0023 (2)	0.7567 (3)	0.1179 (5)	0.0059 (6)
Se1b	0.2511 (2)	0.2514 (2)	0.6242 (5)	0.0061 (6)
Se1c	0.37875 (12)	0.5038 (3)	0.8764 (5)	0.0067 (6)
Se1d	0.88061 (12)	0.5047 (3)	0.8734 (5)	0.0059 (6)
Se2	0.12533 (13)	0.7180 (3)	0.7351 (5)	0.0075 (6)
Se3	0.38468 (13)	0.7398 (3)	0.5056 (5)	0.0090 (7)
Cu1a	0.2375 (2)	0.4640 (4)	0.9976 (6)	0.0224 (9)
Cu1b	0.7709 (2)	0.4158 (4)	0.0472 (5)	0.0173 (8)
Cu2	0.2936 (2)	0.7675 (4)	0.7451 (6)	0.0238 (8)
Cu3a	0.9671 (2)	0.0921 (4)	0.0879 (6)	0.0240 (9)
Cu3b	0.5513 (2)	0.9364 (4)	0.9281 (5)	0.0192 (9)
Cu4a	0.8575 (3)	0.0214 (6)	0.3652 (7)	0.0524 (14)
Cu4b	0.3765 (2)	0.8298 (5)	0.2702 (5)	0.0308 (10)

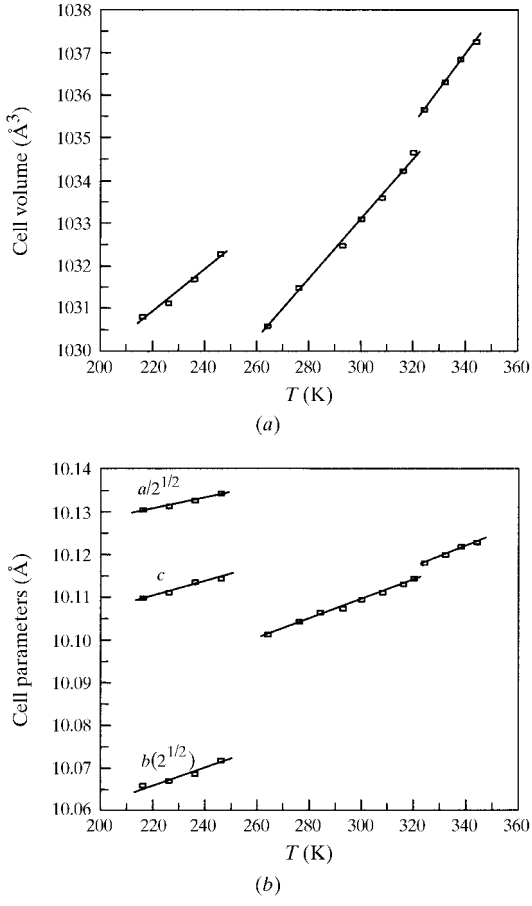

Figure 2
(*a*) Volume and (*b*) cell parameter changes as a function of temperature, clearly showing the two phase transitions.

Table 4
Anisotropic displacement parameters U^{ij} (Å^2) and s.u.s for α-Cu_7PSe_6 ($Pna2_1$, T = 173 K).

The anisotropic displacement factor exponent takes the form: $(-2\pi^2\Sigma_i\Sigma_j U^{ij}a^i a^j h_i h_j)$.

	U^{11}	U^{22}	U^{33}	U^{12}	U^{13}	U^{23}
Se1*a*	0.0065 (9)	0.0074 (10)	0.0039 (11)	0.0010 (7)	−0.0010 (7)	0.0001 (8)
Se1*b*	0.0061 (9)	0.0070 (10)	0.0051 (11)	−0.0010 (8)	−0.0041 (7)	−0.0009 (9)
Se1*c*	0.0085 (9)	0.0057 (10)	0.0059 (10)	0.0014 (9)	−0.0015 (9)	−0.0024 (7)
Se1*d*	0.0069 (9)	0.0062 (10)	0.0046 (10)	0.0022 (9)	0.0002 (9)	−0.0030 (7)
Se2	0.0074 (9)	0.0057 (9)	0.0095 (12)	−0.0009 (8)	0.0013 (10)	0.0016 (7)
Se3	0.0061 (10)	0.0119 (10)	0.0089 (14)	0.0008 (8)	−0.0012 (8)	0.0000 (8)
Cu1*a*	0.0174 (13)	0.0161 (13)	0.034 (2)	−0.0080 (10)	0.0121 (13)	−0.0099 (13)
Cu1*b*	0.0159 (12)	0.0202 (14)	0.0158 (15)	−0.0034 (11)	0.0085 (11)	−0.0042 (12)
Cu2	0.0130 (12)	0.024 (2)	0.034 (2)	−0.0064 (11)	−0.0102 (13)	−0.004 (2)
Cu3*a*	0.025 (2)	0.019 (2)	0.028 (2)	0.0032 (12)	0.0002 (13)	0.0041 (13)
Cu3*b*	0.0209 (15)	0.024 (2)	0.0130 (14)	0.0003 (13)	−0.0044 (12)	−0.0010 (13)
Cu4*a*	0.048 (2)	0.044 (2)	0.065 (3)	0.004 (2)	0.004 (2)	0.040 (2)
Cu4*b*	0.0071 (13)	0.072 (2)	0.0132 (14)	0.0015 (15)	−0.0016 (13)	−0.0114 (15)

showed no interpretable residues, but noise. The twin fractions converged to the 0.3503, 0.0529 (13), 0.0320 (12), 0.0582 (14), 0.3406 (14) and 0.1660 (13) values for *T*1, *T*2, *T*3, *T*4, *T*5 and *T*6, respectively. The final parameters are given in Tables 2–4.

It is interesting to analyze the potential effect of the lack of averaging upon the residual factor final value. Going back to the refinement of β-Cu_7PSe_6, the final residual factor was R = 0.0298 (wR = 0.0334) after averaging the data set according to the point group 23 (Gaudin, Boucher, Petricek *et al.*, 2000). A test refinement without averaging the data yields the much higher R value of 0.0431 (wR = 0.0494). The value of R = 0.046 we obtained for α-Cu_7PSe_6 is therefore reasonably good for a non-averaged data set.

A test of the kinetic effect upon the structure results was also carried out. The data collection previously reported was realised after a cooling rate of 0.1 K min^{-1}. A new data collection has been realised after a faster cooling of 0.5 K min^{-1}. The structure features obtained from that last set are identical to the previous ones, but with a higher residual factor (R = 0.057) and different twinning fractions (0.33, 0.12, 0.09, 0.11, 0.16 and 0.19 for T1, T2, T3, T4, T5 and T6, respectively). The ordering kinetic seems a critical factor to take into account in any measurement for the low-temperature polymorph. Similar effects were observed during the data collections on powders.

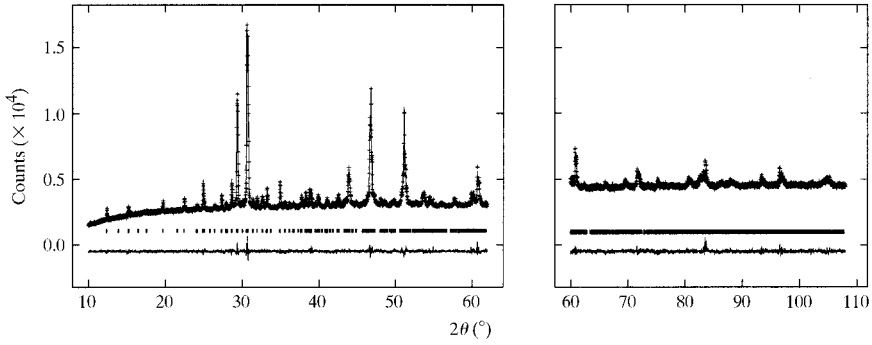

Figure 3
Rietveld refinement test results (observed, calculated and difference diagrams).

2.4. Rietveld refinement

As a final test of our model, a Rietveld refinement was carried out on the X-ray diffractogram collected at 225 K on the Kevex detector-equipped D5000 powder diffractometer. In fact, two histograms were collected with different counting time, from 10 to 64° 2θ and from 60 to 110° 2θ in steps of 0.01° with counting times of 35 and 45 s, respectively. As already discussed, special care was taken to assure complete setting of the ordering, which was checked on the intensities by fast measurements at 30 min intervals. A Le Bail refinement was performed with the *GSAS* program (Larson & Von Dreele, 1994) to establish the lattice parameters, peak profiles (Thompson, Cox and Hasting's function) and background (Chebyschev function). This full pattern-matching refinement led to the global residual profile value R_p = 0.021 and weighted profile value R_{wp} = 0.016. The Rietveld refinement (Rietveld, 1969) was then initiated with the atomic positions and IDPs obtained in the single-crystal refinement (LT2, 173 K), the IDPs being corrected for their temperature effect. Fixing the motif parameters, the refinement converged to R_p = 0.029 (wR_p = 0.020). Finally, freeing the motif parameters let to a very good agreement, with R_p = 0.025 (wR_p = 0.018) and no significant changes on the positions. Details of the refinements are gathered in Table 5 and a plot of the final refinement is presented in Fig. 3.

3. Discussion

In part II of this study (Gaudin, Boucher, Petricek *et al.*, 2000) we showed that in γ-Cu_7PSe_6 (high-temperature form) the Cu^+d^{10} ions are delocalized among the various tetrahedral, triangular and linear low-coordination sites made by the [PSe_6] structure framework and moving along preferential diffusion paths. On lowering the temperature the copper cations preferably occupy the most stable sites along these diffusion paths, hence the phase transition towards β-Cu_7PSe_6. However, the β-Cu_7PSe_6 structure is not fully ordered and a second phase transition occurs at a lower temperature with a complete ordering of the Cu atoms in α-Cu_7PSe_6. As can be seen in Fig. 4, in α-Cu_7PSe_6 the copper positions are still occupying positions along the diffusion paths of the highest-temperature form.

Among the seven independent Cu atoms, five Cu atoms are found in tetrahedral coordination, one Cu atom is in a

Table 5
Powder X-ray data collection and refinement parameters.

Temperature (K)	225	
Wavelengths (Å)	1.54056 and 1.54439	
Diffractometer	Siemens D5000	
2θ (°) range	10–64	60–110
Step (° 2θ); time per step (s)	0.01, 35	0.01, 45
Crystal data		
Chemical formula	Cu_7PSe_6	
Space group	$Pna2_1$	
Cell parameters (Å)	a = 14.32746 (17)	
	b = 7.11827 (7)	
	c = 10.11087 (12)	
Cell volume (Å^3)	1031.1745 (3)	
Z	4	
Refinement		
Structure refinement program	*GSAS*	
Profile function	Thompson *et al.* (1987)	
Profile parameters	X = 6.3 (1), Y = 3.8 (4), A_s = 0.28 (10)	
Background function	Chebyshev	
No. of background parameters	16	3
Full No. of reflections	368	
Full No. of refined parameters	70	
R_p	0.025	
wR_p	0.018	
χ^2	2.191	

triangular site and the remaining Cu atom is linearly coordinated. The fact that the Cu atoms favor tetrahedral sites is in agreement with the usual Cu^+ behavior in chalcogenides, that is, a linear coordination in oxides, a triangular or tetrahedral coordination in sulfides and selenides, and a tetrahedral coordination in tellurides. This trend results from the importance of the metal *s*/*d* orbital mixing and, correlatively, from the d^{10} cation polarization, the higher the electronegativity of the chalcogen, the higher the polarization of the d^{10} cation and the lower the copper coordination (Gaudin, Boucher & Evain, 2000).

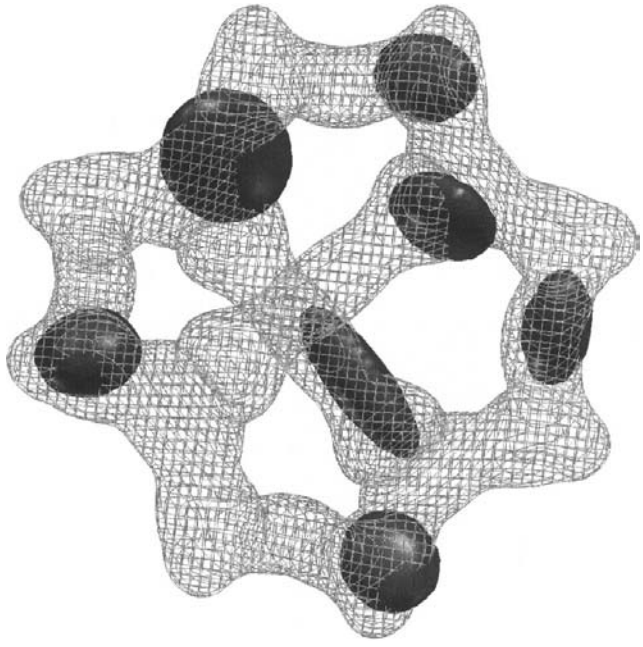

Figure 4
Superposition of the joint probability density isosurfaces calculated for γ-Cu_7PSe_6 at 353 K (frame, at the 0.2 Å^{-3} level) and for α-Cu_7PSe_6 at 213 K (opaque, at the 0.2 Å^{-3} level). Notice that the previously reported density levels for γ-Ag_7PSe_6, γ-Cu_7PSe_6, β-Ag_7PSe_6 and β-Cu_7PSe_6 were in fact in arbitrary units, because of a scaling problem in *JANA*96 and *JANA*98.

As can be seen from Table 6, some [$CuSe_4$] tetrahedral units are rather regular {[Cu1*b*Se_4] unit for instance with Cu—Se distances ranging from 2.439 (6) to 2.592 (6) Å}. In other [$CuSe_4$] tetrahedra, the copper element is strongly displaced toward a selenium face {[Cu4*b*Se_4] unit for instance with three Cu—Se distances around 2.44 Å and one Cu—Se distance at 2.783 (4) Å}. In any case, the average Cu—Se distances of each tetrahedral unit (ranging from 2.487 to 2.553 Å) are close to the value reported by Shannon (1981; 2.475 Å). The average Cu—Se distance is shorter (2.39 Å) in the triangular site and, as expected, even shorter (2.33 Å) in the linear site. As already mentioned, Cu preferentially adopts threefold or fourfold coordination in selenides and the observed linear coordination of Cu4*a* is therefore exceptional. It was not suppressed at the $\beta \rightarrow \alpha$ transition, probably because of incompatibilities. Indeed, all potential triangular or tetrahedral sites surrounding the occupied linear position are already filled or too close to other existing Cu atoms (see Fig. 5). It can therefore be assumed that the selenium linear coordination of copper results from steric effects. The rather large equivalent displacement parameter of Cu4*a* (U_{eq} = 0.052 Å^2) indicates a position disorder around the average location, in agreement with the linear environment frustration. Other steric effects are also probably responsible for some short Cu—Cu contacts found throughout the structure [$d_{Cu3b-Cu4b}$ = 2.525 (6) and $d_{Cu2-Cu1b}$ = 2.559 (7) Å to be compared to d_{Cu-Cu} = 2.54 Å in metallic copper].

The evolution of the volume and cell parameters as a function of temperature presented in Fig. 2 reveals a linear behavior for a given polymorphic form and discontinuities at the phase transitions. Since the cell parameters are order parameters, it is possible to characterize the transitions as first-order transitions. This agrees with MAS NMR observations (Gaudin, Evain *et al.*, 2000). The volume shrinking at the $\gamma \rightarrow \beta$ transition is easily understandable by cessation of the copper large motion found in the ionic conducting γ phase, but the volume increase at the $\beta \rightarrow \alpha$ second transition is more surprising. It could be due to a structure relaxation to minimize the aforementioned steric effects.

4. Conclusions

The crystal structure of α-Cu_7PSe_6 has been solved from X-ray single-crystal diffraction data, the heavy twinning problem being overcome with the help of single-crystal and powder MAS NMR studies. From the three parts of our study, some general trends can be devised for the A_7PSe_6 (A = Ag, Cu) compounds. First, it has been shown that as in other argyrodite compounds the d^{10} cations are mobile in the γ-polymorphs, Ag^+ and Cu^+ moving along well defined diffusion paths joining low-coordination preferential sites. As the temperature decreases, these cations settle in various chalcogen low coor-

Table 6
Main interatomic distances (Å) and su.

PSe_4 sites		$CuSe_2$ sites	
P—Se1*a*	2.194 (5)	Cu4*a*—Se2	2.285 (6)
P—Se1*c*	2.195 (5)	Cu4*a*—Se3	2.370 (7)
P—Se1*b*	2.193 (5)		
P—Se1*d*	2.218 (5)		
⟨P—Se⟩	2.200	⟨Cu4*a*—Se⟩	2.328
$CuSe_3$ sites			
Cu1*a*—Se3	2.369 (3)		
Cu1*a*—Se1*c*	2.380 (5)		
Cu1*a*—Se1*b*	2.417 (5)		
⟨Cu2*a*—Se⟩	2.389		
$CuSe_4$ sites			
Cu1*b*—Se1*d*	2.439 (6)	Cu2—Se1*d*	2.420 (5)
Cu1*b*—Se1*b*	2.511 (4)	Cu2—Se2	2.437 (3)
Cu1*b*—Se3	2.523 (3)	Cu2—Se1*c*	2.600 (5)
Cu1*b*—Se2	2.592 (6)	Cu2—Se3	2.755 (7)
⟨Cu1*b*—Se⟩	2.516	⟨Cu2—Se⟩	2.553
Cu3*a*—Se2	2.405 (6)	Cu3*b*—Se1*a*	2.461 (6)
Cu3*a*—Se1*a*	2.457 (4)	Cu3*b*—Se2	2.476 (6)
Cu3*a*—Se3	2.509 (4)	Cu3*b*—Se1*d*	2.541 (4)
Cu3*a*—Se1*c*	2.575 (7)	Cu3*b*—Se3	2.599 (4)
⟨Cu3*a*—Se⟩	2.487	⟨Cu3*b*—Se⟩	2.519
Cu4*b*—Se1*b*	2.413 (5)		
Cu4*b*—Se1*a*	2.447 (6)		
Cu4*b*—Se3	2.467 (7)		
Cu4*b*—Se2	2.783 (4)		
⟨Cu4*b*—Se⟩	2.528		
Shortest Cu—Cu contacts in α-Cu_7PSe_6			
Cu3*b*—Cu4*b*	2.525 (6)		
Cu2—Cu1*b*	2.559 (7)		
Cu4*a*(linear coordination)—Cu distances in α-Cu_7PSe_6			
Cu4*a*—Cu4*b*	2.689 (6)		
Cu4*a*—Cu1*b*	2.706(7)		
Cu4*a*—Cu2	2.899 (6)		

dination sites. For silver, the localization is realised through only one transition, with one twofold-, three threefold- and three fourfold-coordinated Ag atoms. For copper, an initial localization is obtained through a first transition with approximately one twofold-, two threefold- and four fourfold-coordinated Cu atoms. That localization is only partial and movements are still operating as indicated by the high DWFs. Then a full localization is reached with one twofold-, one threefold- and five fourfold-coordinated Cu atoms. The behavior difference is to be related to the d^{10} element stability in low coordination environment, copper being less prone to lower coordination sites than silver, especially at low temperature. For Ag atoms, the final stage is obtained in one step, but for copper the situation is more complicated and the final stage is obtained in two steps, the twofold and threefold sites becoming less and less favorable as the movement between the sites is reduced.

APPENDIX *A*

A1. Averaging equivalent reflections with twinning

In the case of a merohedral or a pseudo-merohedral twinning the critical step for the merging of symmetry-equivalent reflections consists of determining the symmetry operations (S_i) of the point group (**S**) that can be used. Indeed interferences should not occur between domains in the calculation of the structure factors.

For completely overlapping reciprocal lattices the structure factor is calculated using *JANA*2000 from

$$F^2(\mathbf{H}) = \nu_1 F^2(\mathbf{H}T_1) + \nu_2 F^2(\mathbf{H}T_2) + \ldots + \nu_m F^2(\mathbf{H}T_m), \quad (1)$$

with $\mathbf{H} = (h,k,l)$, T_m the mth twinning operation, ν_m the fractional volume of the mth domain generated by the symmetry operation T_m ($\nu_m = V_m/V_{\rm tot}$). Notice that the fractional volumes are not usually identical.

Let $\mathbf{H}S$ be the set of symmetry-equivalent reflections of **H**, that is $F^2(\mathbf{H}S) = F^2(\mathbf{H})$. For the S_i symmetry operation, the structure factor of the twinned crystal takes the form

$$F^2(\mathbf{H}S_i) = \nu_1 F^2(\mathbf{H}S_iT_1) + \nu_2 F^2(\mathbf{H}S_iT_2) + \ldots + \nu_m F^2(\mathbf{H}S_iT_m).$$

The necessary condition for S_i to be a symmetry element of the twinned structure factor is therefore

$$S_iT_k = T_kS_j, \text{ that is } S_j = T_k^{-1}S_iT_k \quad (2)$$

for all twinning reflections. Only these symmetry operations can be used for merging symmetry-equivalent reflections. This is the condition used in *JANA*2000 for selecting the operations.

According to group theory, S is a subgroup of the apparent group $A = ST$, with T the set of twinning operations and ST the right coset of S in A with respect to T. The set of elements of S which fulfil the condition (2) is an invariant subgroup S' of A. In fact, condition (2), $S_iT_m = T_mS_j$, specifies that the left and right cosets of S' are identical, the definition of a normal or invariant subgroup. The invariant subgroup S' consists of complete classes of A. Thus, only complete classes of operations of A which belong to S can be used for merging the symmetry-equivalent reflections.

In the case of α-Cu_7PSe_6 the three classes of $mm2$ are $\{E\}$, $\{2\}$ and $\{m[110], m[1\bar{1}0]\}$, and in the $\bar{4}3m$ apparent point group

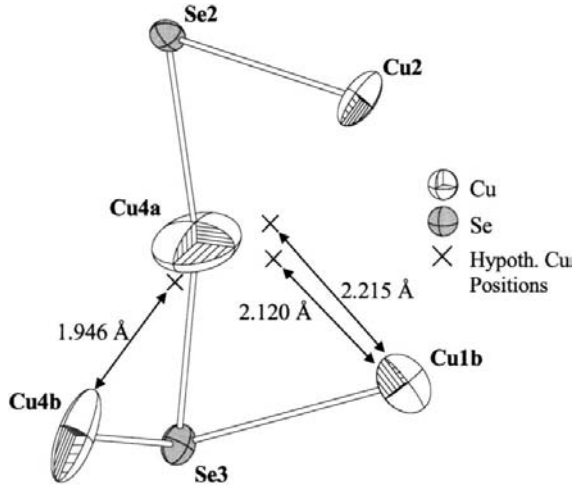

Figure 5
Linear coordination of Cu4. Potential non-linear sites are indicated by crosses along with their distances to filled copper sites, illustrating the Cu4 frustration.

the twofold axis and mirror plane classes contain three and six elements, respectively. Thus, $\{E\}$ of $mm2$ is the only complete class of $\bar{4}3m$ and thus E is the only symmetry operation that can be used for merging. For β-Cu_7PSe_6 (Gaudin, Boucher, Petricek *et al.*, 2000), the apparent group was also $\bar{4}3m$, but the point group domain was different, *i.e.* 23 (space group $P2_13$). 23 is made up of complete classes of $\bar{4}3m$, thus all the operations of 23 can be used for merging the symmetry-equivalent reflections.

It is worth noticing that when all the operations of the domain point group can be used, the twinning operations can be introduced after the data set treatment. This is always the case for merohedral twinning (see below).

A2. Twinning type and averaging

From the definition of the merohedral and pseudo-merohedral twinning (complete overlapping of the reciprocal lattices of the twin components, twin index 1; Herbst-Irmer & Sheldrick, 1998; Koch, 1992) let us discuss the possibility for the merging of symmetry-equivalent reflections. Notice that in the case of a twin index greater than 1, the overlapping spots make a subset which is a merohedral or pseudo-merohedral twin and the averaging of this subset can be handled in the same way.

A2.1. Twins by merohedry. The twin operation belongs to the point group of its vector lattice. Two possibilities occur:

(i) The twin operation belongs to the Laue class of the crystal. The twin can then be described as an inversion twin with the twin operation being the inversion (racemic twin). The apparent point group, the Laue group, is generated by multiplying the domain point group by the $\{E,i\}$ group. As any symmetry operation commutes with the inversion operation ($S_i i = iS_i$), the left and right cosets of the point group domain with respect to i are the same. Therefore, any domain point group is an invariant subgroup of the corresponding Laue group and all the operations of the domain point group can be used for the averaging of the symmetry-equivalent reflections.

(ii) The twin operation belongs to the holohedry corresponding to the domain point group, but not to the Laue class of the crystal. This is only possible for trigonal, tetragonal, hexagonal and cubic crystal systems. All point groups are complete classes of the holohedry, thus they are invariant subgroups of the holohedry and once more their symmetry operations fulfill condition (2). This is the case for β-Cu_7PSe_6 (Gaudin, Boucher, Petricek *et al.*, 2000).

A2.2. Twinning by pseudo-merohedry. The twin operation belongs to a higher crystal class than the class of untwinned crystal. For a complete overlapping of the domain reciprocal lattices the metric symmetry should be compatible with the higher symmetry. There is no general relation between the apparent and the domain point groups when considering condition (2). For the overlapping reflections of α-Cu_7PSe_6 only multiple measured reflections can be averaged since no symmetry operations of $mm2$ except E belong to an invariant subgroup of $\bar{4}3m$.

References

Becker, P. J. & Coppens, P. (1974). *Acta Cryst.* A**30**, 129–147.

Creagh, D. C. & McAuley, W. J. (1992). *International Tables for X-ray Crystallography*, Vol. C, edited by A. J. C. Wilson, ch. 4.2. Dordrecht: Kluwer Academic Publishers.

Evain, M., Boucher, F., Gaudin, E., Petricek, V. & Taulelle, F. (1998). *Acta Cryst.* B**54**, 376–383.

Gaudin, E., Boucher, F. & Evain, M. (2000). Submitted.

Gaudin, E., Boucher, F., Petricek, V., Taulelle, F. & Evain, M. (2000). *Acta Cryst.* B**56**, 402–408.

Gaudin, E., Evain, M., Boucher, F. & Taulelle, F. (2000). In preparation.

Herbst-Irmer, R. & Sheldrick, G. M. (1998). *Acta Cryst.* B**54**, 443–449.

Koch, E. (1992). *International Tables for Crystallography*, Vol. C, edited by A. J. C. Wilson, ch. 1.3. Dordrecht: Kluwer Academic Publishers.

Larson, A. C. & Von Dreele, R. B. (1994). *GSAS*. Report LAUR 86-748. Los Alamos National Laboratory, USA.

Le Bail, A., Duroy, H. & Fourquet, J. L. (1988). *Mater. Res. Bull.* **23**, 447–452.

Maslen, E. N., Fox, A. G. & O'Keefe, M. A. (1992). *International Tables for Crystallography*, Vol. C, edited by A. J. C. Wilson, ch. 6.1. Dordrecht: Kluwer Academic Publishers.

Petricek, V. & Dusek, M. (1998). *JANA*2000. Institute of Physics, Academy of Sciences of the Czech Republic, Prague, Czech Republic.

Rietveld, H. M. (1969). *J. Appl. Cryst.* **2**, 65–71.

Shannon, R. D. (1981). *Structure and Bonding in Crystals*, edited by M. O'Keeffe and A. Navrotsky, Vol. II, pp. 53–70. New York: Academic Press.

Thompson, P., Cox, D. E. & Hastings, J. E. (1987). *J. Appl. Cryst* **20**, 79–83.